FUNDAMENTALS & APPLICATIONS

CHEMELECTROCHEM

ANALYSIS & CATALYSIS, BIO & NANO, ENERGY & MORE

Accepted Article

Title: Polarization resistance-free Mn3O4-based electrocatalysts for the oxygen reduction reaction

Authors: Yafei Fan, Yanlin Wu, Xing Huang, Guylhaine Clavel, Patrick Amsalem, Norbert Koch, and Nicola Pinna

To be cited as: *ChemElectroChem* 10.1002/celc.201800477

Link to VoR: http://dx.doi.org/10.1002/celc.201800477

A Journal of

ChemPubSoc Europe

WILEY-VCH

www.chemelectrochem.org

Polarization resistance-free Mn_3O_4-based electrocatalysts for the oxygen reduction reaction

Yafei Fan,[a] Yanlin Wu,[a] Xing Huang,[b] Guylhaine Clavel,[a] Patrick Amsalem,[c] Norbert Koch,[c] Nicola Pinna[a]*

[a] Institut für Chemie and IRIS Adlershof Humboldt-Universität zu Berlin Brook-Taylor-Str. 2, 12489 Berlin, Germany

[b] Department of Inorganic Chemistry, Fritz Haber Institute of the Max Planck Society, Berlin, Germany

[c] Institut für Physik and IRIS Adlershof, Humboldt-Universität zu Berlin, Brook-Taylor-Str. 6, 12489 Berlin, Germany

*E-mail: nicola.pinna@hu-berlin.de

Abstract

Transition metal oxides have been proposed as a possible replacement of Pt for the electrocatalytic oxygen reduction reaction (ORR), however the low intrinsic conductivity makes their application in electrocatalysis challenging. In this work, we demonstrate that atomic layer deposition (ALD) is capable to overcome this problem by coating conductive carbon nanotubes substrates with a conformal Mn_3O_4 layer of just few-nm in thickness. The deposition parameters have been optimized in terms of thickness and crystallite sizes in order to produce a material exhibiting catalytic efficiency close to the one of carbon-supported Pt particles and low polarization costs. The current densities recorded in linear sweep voltammetry prove that the Mn_3O_4 coating leads to a substantial increase of the catalytic efficiency, compared to uncoated carbon nanotubes, and was also higher than other manganese-based catalysts reported so far. The sample prepared from only 50 ALD cycles (e.g. coating thickness of ~2 nm) shows the best compromise between catalytic efficiency, with an onset potential at 0.867 V (vs. RHE), and good conductivity of the electrode materials minimizing polarization. Indeed, the Tafel plots exhibit a similar slope than Pt/C demonstrating that the Mn_3O_4/CNTs reduce oxygen in a one-step four electrons mechanism and with a similar kinetics as Pt-based electrocatalysts. Moreover, the current density keeps at 80% even after 12 h at 0.58 V displaying therefore a higher stability than Pt-based catalysts. These findings are attributed to the few nm-thick conformal and catalytic active coating obtained by atomic layer deposition, which also protects the underneath CNT substrate from corrosion.

Keywords

Oxygen reduction reaction (ORR), atomic layer deposition (ALD), carbon nanotubes (CNTs) and manganese oxide

Introduction

Oxygen reduction reaction (ORR) which is the key process for many oxygen-based energy conversion and storage devices, such as regenerative fuel cells and metal-air batteries, has gained great interest since the last decade. The difficulty of ORR is that two or four electrons have to be transferred at once for the reduction of one oxygen molecule to peroxide O_2^{2-} or oxide O^{2-} respectively[1] which requires a high overpotential and subsequently decreases the efficiency of the energy conversion devices. To date the most efficient catalysts are noble metals such as platinum[2] which increase the costs of devices significantly. Thus, scientists are trying to replace platinum with abundant transition metals displaying the required high catalytic activity for the ORR. Manganese oxides have been proposed due to their good catalytic activities. Ketjenblack carbon supported amorphous manganese oxides nanowires showed remarkable catalytic performance for the ORR and was further applied in metal-air batteries.[3] The ORR catalytic performance of bifunctional MnO_2 was optimized by investigating the relationship of structure and property in alkaline media.[4] Binary catalyst combining Au for the 2-electrons reduction of oxygen to peroxide and MnO_x for the reduction of peroxide species to oxide ions has been reported by EI-Deab et al.[5] Additionally, Mn_3O_4 is an active catalyst for several redox reactions due to its polymorphism and coexistence of mix-valence species.[6] However, the low conductivity as well as dissolution and agglomeration of the Mn_3O_4 reduce the catalytic activity during the electrochemical reduction of oxygen.[7]

One strategy to overcome the intrinsic low conductivity of Mn_3O_4 is to deposit nm-thick films or nm-sized particles onto highly conductive substrate such as carbon. Certainly, carbon is the most common conductive material used in energy conversion and storage devices such as Li-ion batteries and proton exchange membrane fuel cells.[8] The combination of carbon and noble metals is commonly used for the fabrication of ORR catalysts, where carbon provides the required high surface area to the electrodes while preserving a good electronic conductivity of the composite electrode material, and the noble metal nanoparticles provide the catalytic centers.[9] However, Pt-based catalysts are known to gradually degrade over time because of surface oxides and particle dissolution and aggregation, especially in the alkaline electrolytes used for alkaline fuel cells.[10] Several carbon nanostructures have been tested including carbon black, fibers, nanotubes and graphene. Carbon nanotubes (CNTs) are among the preferred ones because they not only act as a good conductive substrate, but also provide large accessible surface area due to the nanostructured 1-D geometry.[11]

Due to the high aspect ratio of CNTs, line of sight deposition methods such as physical and chemical vapor deposition can not conformally coat the CNTs surface. Atomic layer deposition (ALD), on the other hand, has been shown to provide conformal coating of nanostructures displaying aspect ratio of 100 and larger, such as DRAM trenches,[12] CNTs,[13] and mesoporous materials.[14] In the ALD process, the distinct precursors vapor only chemisorb onto functional group present on the surface of the substrate alternately. The precursors excess as well as byproducts are removed by the following purging step in each half cycle.[15] The design of this process avoids different precursors to react with each other in the gas phase, subsequently avoiding chemical vapor deposition (CVD)-like processes. Therefore, ALD can be used to deposit conformal thin films onto nanostructured and high aspect ratio substrates.[16] ALD has been widely used in the last decade for the synthesis of nanostructured materials for energy conversion and storage,[17] for example tungsten oxide for

water splitting,[18] NiO and Sb_2S_3 for photoelectrocatalytic water splitting[19] and especially ALD prepared MnO using $Mn(EtCp)_2$ and H_2O as precursors on glassy carbon for oxygen evolution reaction (OER) and ORR.[20] However, the relative low surface area of glassy carbon and the fast and high corrosion of the electrodes by the electrolytes limited the efficiency and stability of the electrodes and their catalytic performances.

In this work, Mn_3O_4 was deposited onto CNTs using ALD by the novel manganese oxide ALD process, which was recently developed in our group.[21] The Mn_3O_4/CNTs system introduced in this work exhibiting a combination of high catalytic activity, low polarization and high stability of the manganese oxide thin films, and good conductivity and large surface area of the carbon nanotube structure, show to reduce oxygen following the same mechanism, similar kinetics and with even an improved stability compared to Pt-based catalysts.

Results and discussion

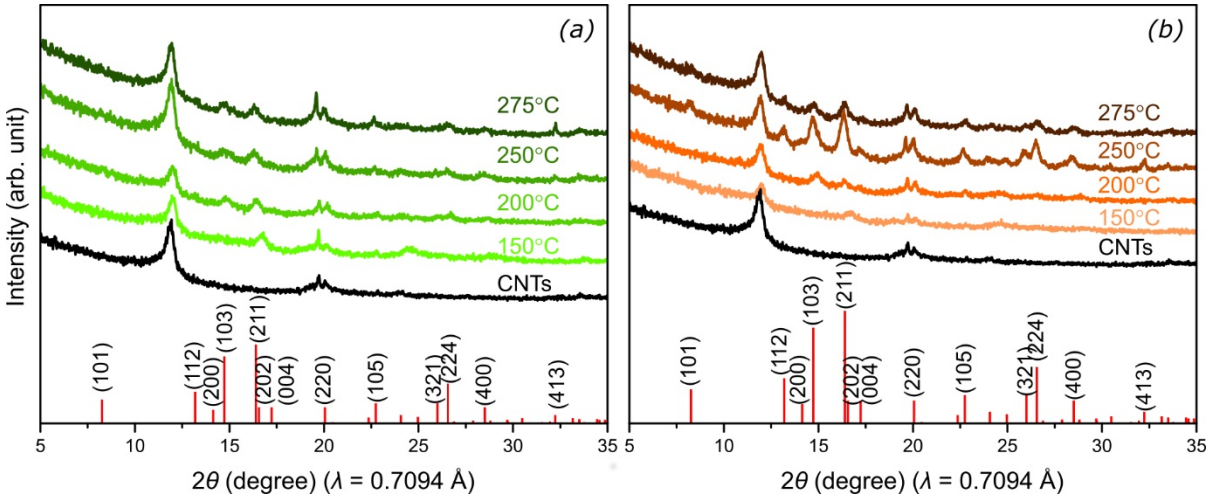

Figure 1. X-ray diffraction of CNTs and Mn_3O_4/CNTs, Mn_3O_4 was deposited at different temperatures for 100 *(a)* and 200 ALD cycles *(b)*. Black curves are the measurement of pure CNTs as reference, the color shifted from light to dark are corresponding to the deposition with the increased temperatures, 150°C, 200°C, 250°C and 275°C. Bars reference pattern of Hausmannite.

In our previous work, Mn_3O_4 was deposited by ALD using $MeCpMn(I)(CO)_3$ and O_3 as precursors. It was shown that this new process could be applied in a large range of deposition temperatures (from 100°C to 275°C).[21] In general, the deposition temperature can significantly affect the materials deposited. For example, if the temperature is too low, one precursor could condense onto the substrates surfaces and would not be completely removed during the purge and therefore react with the second precursor causing additional CVD-like deposition. Conversely, if the temperature is too high, thermal decomposition of the precursors can take place leading to a CVD component to the process, an increase of the growth per cycle and a lower film quality. Moreover, the desorption of active surface species[16a] at high temperature can cause a decrease of the growth per cycle. Both cases would result in a non-conformal growth, and the films deposited under non-ideal ALD conditions would exhibit different morphological, physical (e.g. mechanical) and chemical properties, which would affect the catalytic activity and stability of the electrode material. Therefore, we

investigate first the chemical, structural and morphological properties of CNT-supported Mn_3O_4 as a function of the deposition temperature and number of ALD cycles.

Mn_3O_4 was deposited at four different temperatures between 150°C and 275°C. X-ray diffraction (XRD) is used to characterize the crystal structure of the Mn_3O_4 coatings onto the CNTs (**Figure 1**). The black curves from both panels are the reference diffractograms acquired from pure CNTs before ALD. The peaks at 11.92° and 20° belong to the pure CNTs. The reflections in the patterns of the composites situated at 8.3°, 13.2°, 14.7°, 16.4°, 26.6° and 28.5° correspond to the (101), (112), (103), (211), (224), (400) reflections of Mn_3O_4 hausmannite (JCPDS Card No. 24-734), respectively (some of them are weak and/or can be observed only in patterns recorded from thick samples deposited at high temperature).[21] The most intense reflections centered at 14.7° and 16.4° increase with the increasing of the deposition temperatures pointing to an increase of the crystallite size. The reflections attributed to the hausmannite phase are sharper and more clearly resolved for samples deposited with large number of deposition cycles (**Figure 1b**). These results prove that although the deposition temperature and number of cycles do not influence the crystal phase, they do influence the crystallite size.

The manganese oxide coatings deposited at low temperature (below 200°C) are smooth and amorphous (**Figure SI-1**) while an increase of the deposition temperature at or above 200°C leads to a polycrystalline film (**Figure 2**).[21] The influence of the number of ALD cycles on the morphology of the Mn_3O_4 coating was investigated by high resolution transmission electron microscopy (HRTEM) (**Figure 2**). In the upper row the increase of the crystallites from 2-3 nm for 50 ALD cycles (**Figure 2a**) to around 4-5 nm for 100 ALD cycles (**Figure 2b**) and to around 8-10 nm for 200 ALD (**Figure 2c**) is clearly visible. In the HRTEM images, lattice fringes of the graphitized walls of the multiwalls CNTs (short red lines) and additional fringes of the hausmannite phase can be discerned (**Figure 2d-f**). The insets show the power spectra of the regions indicated by the black circles in the phase contrast images. In the 50 ALD cycles sample, due to the small crystallite size, it is difficult to select single crystallites, so the power spectrum shows reflections from several particles, but each reflection can be attributed to the hausmannite structure. Additionally, a pair of spots indicated by small red circles are attributed to the graphitized walls. For larger number of ALD cycles single crystallites can be selected and their power spectra (Insets of **Figure2e,f**) display hausmannite particles aligned along the [331] and [120] zone axis, respectively. All in all, HRTEM studies demonstrate a homogeneous coating of the CNTs with hausmannite particles randomly oriented and with sizes linearly depending on the number of ALD cycles.

10.1002/celc.201800477

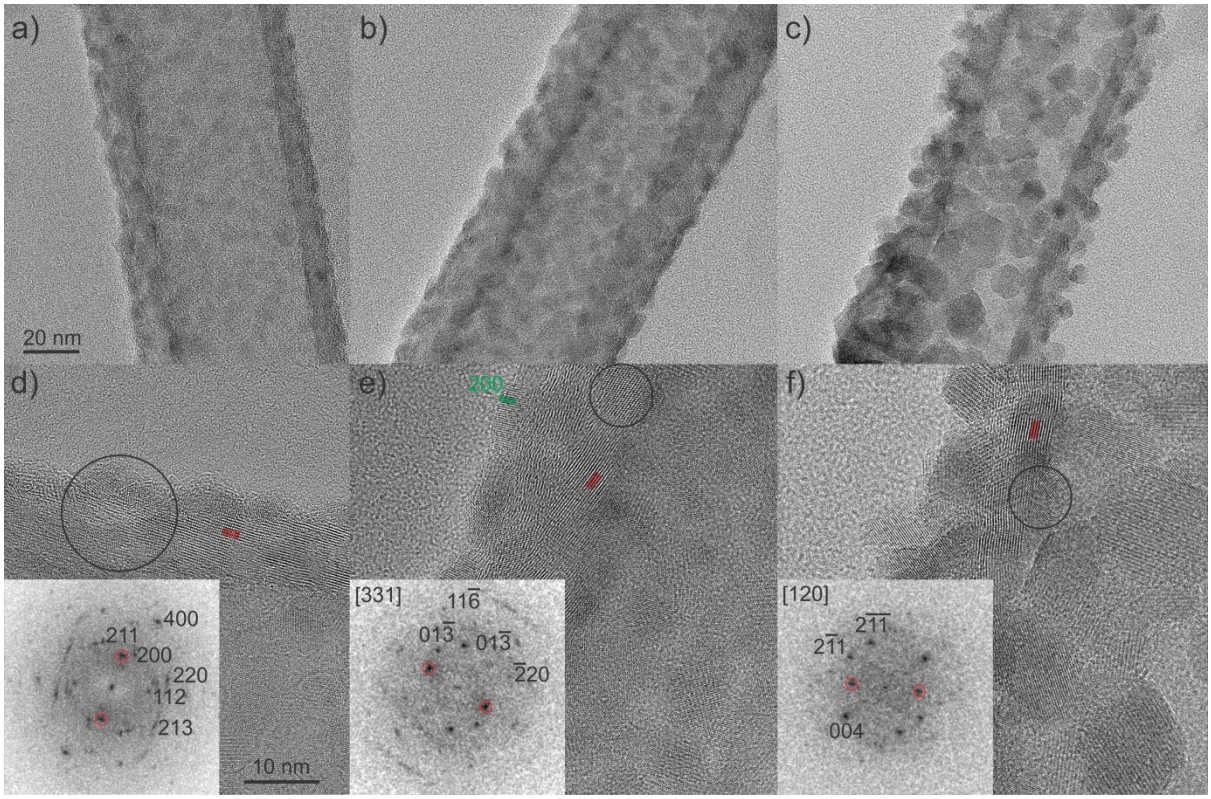

Figure 2. High resolution transmission electron micrographs of Mn_3O_4/CNTs after 50 (a,d), 100 (b,e) and 200 (c,f) cycles at 275°C. The insets show the power spectra of the regions selected by a black circle in the corresponding panel. The scale bars are 20 nm for the upper row and 10 nm for the lower row. (cf. **Figure SI-2** for a higher resolution version of the figure)

The chemical surface composition of the Mn_3O_4 nanoparticles is characterized by X-ray photoelectron spectrometry (XPS) (**Figure 3**). Two peaks at 653.6 eV and 642.1 eV are corresponding to the binding energy of Mn $2p_{3/2}$ and Mn $2p_{1/2}$, respectively. No difference in binding energies is detected for samples deposited at different temperatures, moreover, the energy difference ΔE_{2p} between $2p_{3/2}$ and Mn $2p_{1/2}$ stays constant at 11.6 eV (**Figure 3a**). This value is the same as reported for previous studies on hausmannite.[22] **Figure 3b** displays the Mn 3s core levels whose multiplet splitting ΔE_{3s} is a very sensitive signature of the oxidation state. For the films deposited at or above the 200°C, ΔE_{3s} shows no significant difference and amounts to ca. 5.65 eV $\pm$ 0.05 eV, consistently with the range of value reported for Mn_3O_4.[23] Only for the film prepared at 150°C, we observe a decrease ΔE_{3s} to 5.1 eV which suggests a higher oxidation state of Mn at the film surface. From the TEM and XPS results, we note that the deposition temperature only influences the morphology and the crystallinity, but has no effect on the phase and chemical composition of Mn_3O_4, at least for samples prepared at or above 200°C.

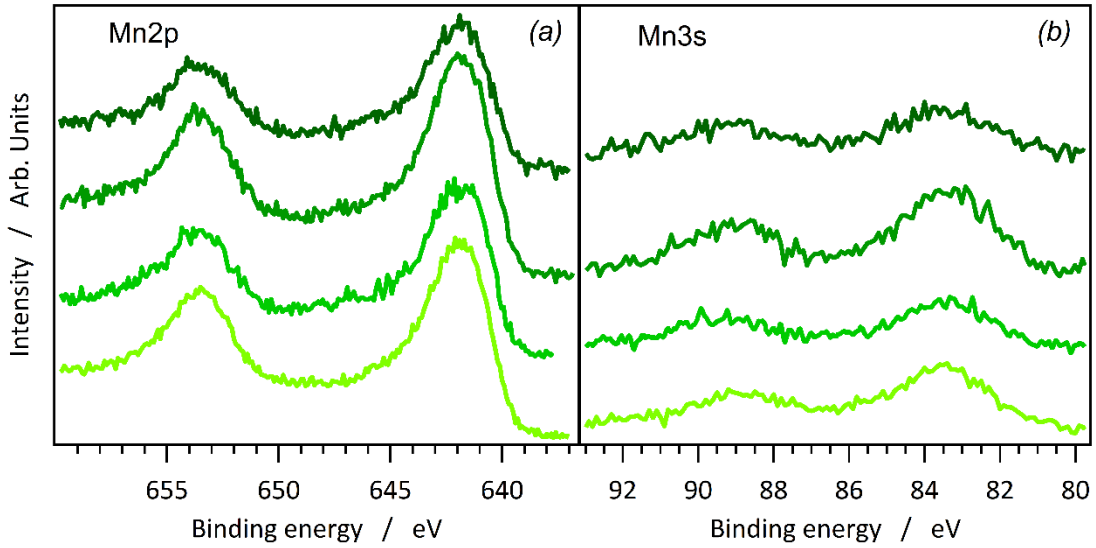

Figure 3. X-ray photoelectron spectrometry (XPS) of Mn_3O_4/CNTs after 100 cycles of Mn_3O_4 ALD, binding energy of Mn 2p *(a)* and Mn 3s *(b)*. The color shifted from light to dark green are corresponding to the deposition with the increased temperatures, 150°C, 200°C, 250°C and 275°C.

The catalytic activity of Mn_3O_4/CNTs for ORR was studied by rotating disk electrode (RDE) in alkaline solution (0.1 M KOH). Linear sweep voltammetry (LSV) of Mn_3O_4/CNTs after 100 ALD cycles was first established on RDE with a spin rate of 1600 rpm (**Figure 4a**). The same experiment was also demonstrated with bare CNTs and a mixture of Mn_3O_4 nanoparticles and CNTs as a reference. These LSV curves show, that bare CNTs exhibit limited catalytic activity for ORR as already reported in some previous studies.[24] However, Mn_3O_4 coated CNTs exhibit an enhanced catalytic activity, even compared to a physical mixture, due to the better coating quality and the more stable chemical binding between the Mn_3O_4 film and CNTs surface. Indeed, the onset potential is increased from 0.747 V to 0.877 V, and the current density in the diffusion limited region also increases notably. The shapes of LSV curves indicate that the catalytic mechanism of CNTs and Mn_3O_4/CNTs are different. The curve of bare CNTs clearly shows two steps of reduction of oxygen molecules with a plateau between 0.597 V and 0.207 V. This result is in agreement of the work by Gong *et al*. reporting that the first stage starts from 0.777 V, which corresponds to the reduction of O_2 to HO_2^- as a two-electron transfer reduction (eq. 1), followed by another two-electron transfer which reduce HO_2^- to OH^- (eq. 2).[25]

$$O_2 + H_2O + 2e^- \rightarrow HO_2^- + OH^- \qquad \text{eq. 1}$$

$$HO_2^- + H_2O + 2e^- \rightarrow 3\ OH^- \qquad \text{eq. 2}$$

This two steps reduction is confirmed by the calculation of electron transfer number by Koutechy-Levich equation from LVS leading to an electron transfer number of 2.68. The calculation details and equations are explained in the experimental section.

10.1002/celc.201800477

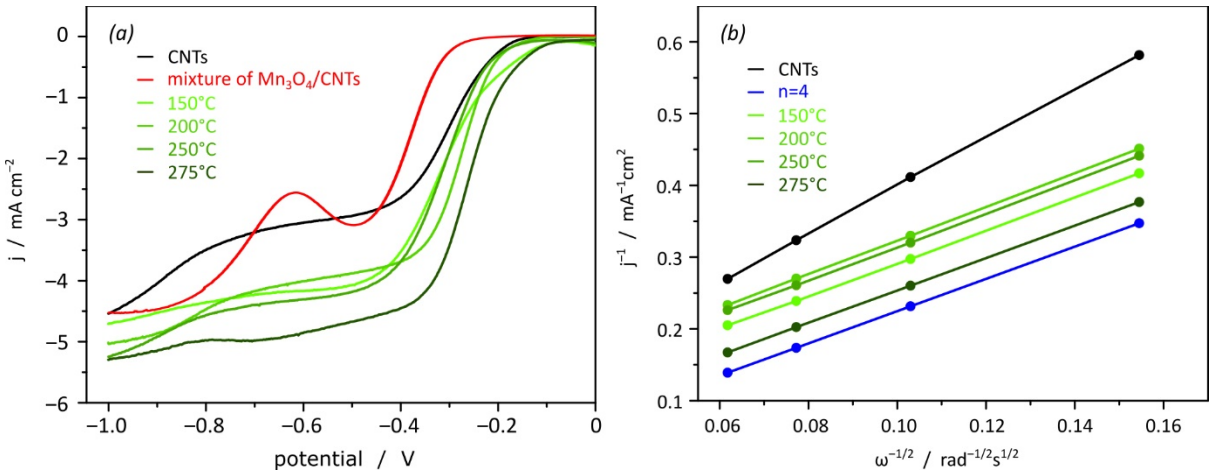

Figure 4. Catalytic electrochemical characterization of Mn_3O_4/CNTs after 100 ALD cycles of Mn_3O_4. *(a)* LSV of Mn_3O_4/CNTs in O_2-Saturated 0.1 M KOH at 25°C with increasing deposition temperature (150°C, 200°C, 250°C and 275°C, light green to dark green curves). Bare CNTs (black) and the mixture of Mn_3O_4/CNTs (red) are used as reference. The scan rate was 10 mV s^{-1}. *(b)* Calculated electron transfer number (*n*) of Mn_3O_4/CNTs with increased deposition temperature (150°C (*n* = 3.93), 200°C (*n* = 3.83), 250°C (*n* = 3.87) and 275°C (*n* = 3.98), light green to dark green curves) during ORR at 0.39 V (vs. RHE). Pure CNTs (black *n* = 2.68) and theoretical values (blue *n* = 4) are used as references.

In contrast to bare CNTs, the ALD-coated samples exhibit a one-step reduction mechanism with calculated electron transfer number close to 4 for all the samples, independently of the deposition temperature (**Figure 4**). Additionally, the Mn_3O_4/CNTs composite do exhibit higher catalytic activity compared to bare CNTs. The sample prepared at 275°C displays an onset potential (0.867 V) which is more than 100 mV lower than bare CNTs and almost double current density than bare CNTs in the diffusion limited region. On the other hand, it is observed that the deposition temperature does influence the catalytic activity. Indeed, the sample prepared at 275°C displays the highest catalytic activity, the highest onset potential (0.867 V) and the largest current density in the diffusion limited region (**Figure 4**). One of the factors influencing the ORR activity is the morphology of the active material as it was already reported for Mn_3O_4 nanoparticles supported on graphene.[7] If we consider the evolution of the morphology and crystallinity of our catalyst determined by TEM and XRD studies as a function of the temperature (see above), it can be concluded that the best catalytic performances are obtained for the highly crystalline and particulate-like Mn_3O_4 coatings. Therefore, for further studies the deposition temperature was fixed at 275°C.

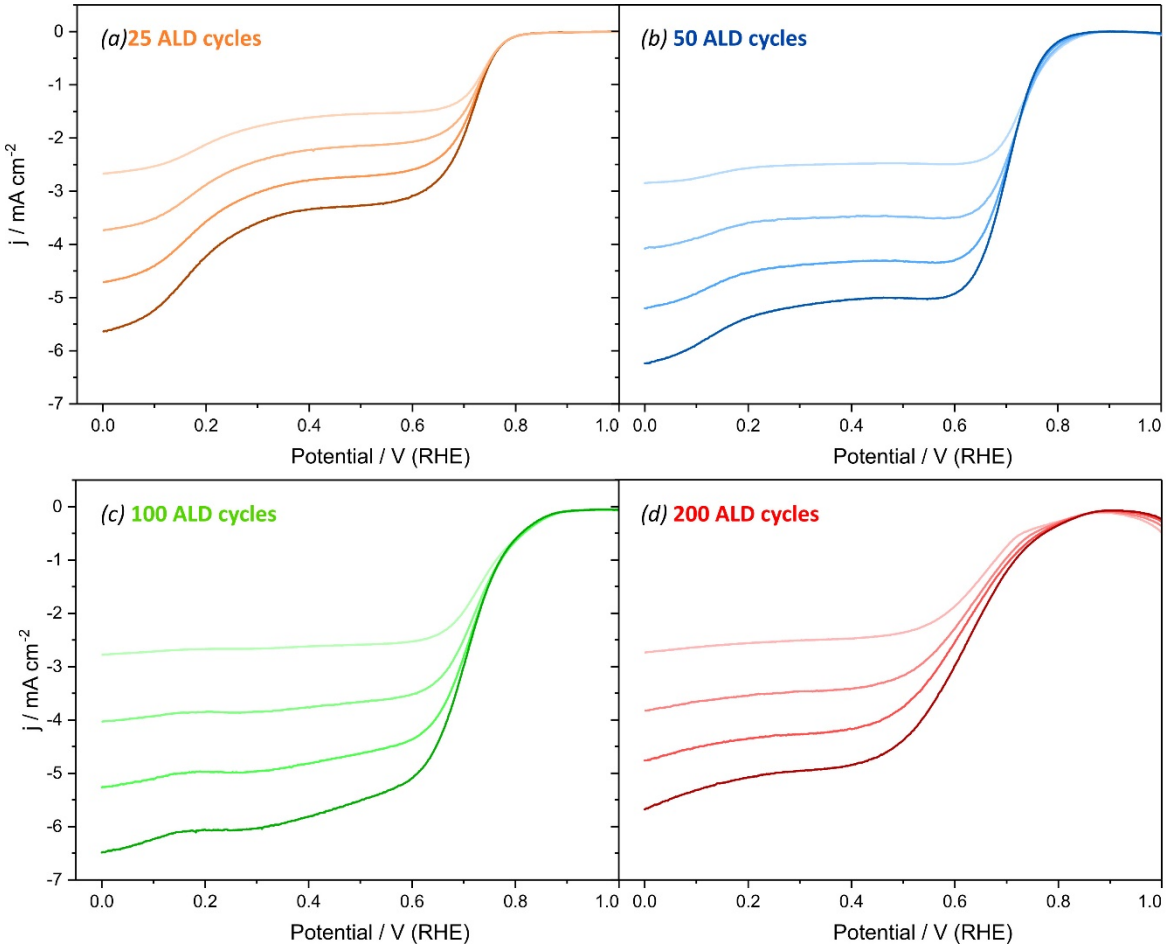

Figure 5. LSV of Mn_3O_4/CNTs on RDE in O_2-Saturated 0.1 M KOH at 25°C for different ALD cycle numbers, *(a)* 25 cycles; *(b)* 50 cycles; *(c)* 100 cycles; *(d)* 200 cycles, at 275°C with 10 mV s^{-1} scan rate. The spin rate of the electrodes increases with the color from light to dark (400 rpm, 900 rpm, 1600 rpm and 2500 rpm).

The catalytic activity also depends on the thicknesses of the Mn_3O_4 coating. Mn_3O_4/CNTs synthesized with 25, 50, 100 and 200 ALD cycles were used as working electrodes for RDE experiments under different rotating speed (**Figure 5**). The sample with 50 and 100 ALD cycles exhibits the best catalytic activity and the highest current density, approx. 5 mA cm^{-2} in the diffusion limited region at 1600 rpm which is higher than in previous reports.[26] The half-wave potentials at 1600 rpm are 0.71 V (**Figure 5b,c**), which is similar to the one reported for carbon supported Mn-Co nanoparticles,[27] and better than the ones reported for pure manganese oxides synthesized by other methods.[7, 20, 26, 28] The linear relationship between j^{-1} and $\omega^{-1/2}$ corresponds to a typical diffusion limited reaction, and the electron transfer number is close to 4 between 0.5 V and 0 V, pointing to a four-electron pathway of oxygen reduction (**Figure SI-4**):

$$O_2 + 2H_2O + 4e^- \rightarrow 4OH^- \qquad \text{(Eq. 3)}$$

The samples prepared with 25 and 200 ALD cycles show slightly lower catalytic activity than the one with 100 cycles in term of the current density in the diffusion-limited region (**Figure 5a and d**). The

low amount of material and the incomplete coating (cf. **Figure SI-3**), can explain the lower activity of the sample with 25 ALD cycles and the quasi two step reaction from the LSV study (**Figure 5a**). On the other hand, an increase of the electrode resistance due to a thicker Mn_3O_4 layer is the reason of the lower activity of the sample with 200 ALD cycles (**Figure 5d**).

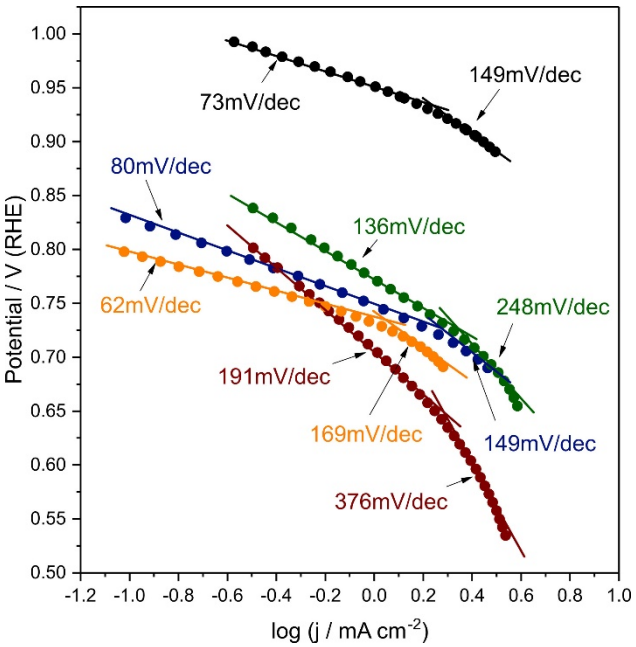

Figure 6. Tafel plot of Mn_3O_4/CNTs prepared at 275°C after 25 (orange), 50 (blue), 100 (green) and 200 (red) ALD cycle numbers and Pt/C as reference (black).

To quantitatively compare the kinetics of the different samples, the Tafel plots are derived from the LSVs (**Figure 6**). As expected all the samples, including the reference Pt/C, display a two-step Tafel slope.[29] The sample with 25 and 50 ALD cycles exhibits the lowest slopes, which are lower than other reported manganese oxide materials[7,26], and comparable or even better to the ones of the reference Pt/C (73-149 mV dec^{-1}) pointing to a low resistance polarization of our material. However, the sample with 25 ALD cycles displays a lower current density than the other samples due to the incomplete coating of the CNTs support (cf. **Figure SI-3**). The sample with 50 cycles shows higher current density and also low Tafel slopes. On the other hand, although the sample with 100 ALD cycle shows similar current density (cf. **Figure 5**), the Tafel slopes are larger (136-248 mV dec^{-1}). The sample with 200 ALD cycles shows an even steeper slope (191-376 mV dec^{-1}). The increasing of the Tafel slopes with the number of ALD cycles (100 and 200), so with the thickness of the coating, is attributed to an increased polarization due to the decreasing of the conductivity of the electrode induced by a thicker and continuous coating with a low conductive material. For the thinnest coatings (25-50 ALD cycles), the similar Tafel slopes as for Pt/C point to similar reaction kinetics and ORR mechanism.

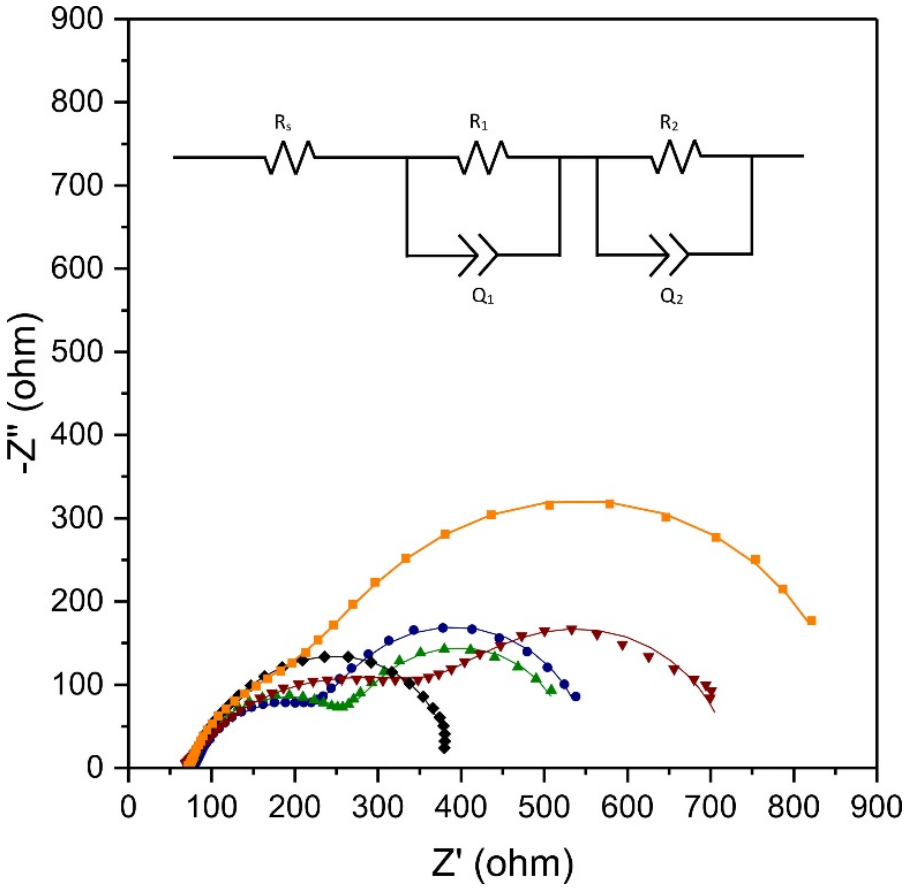

Figure 7. EIS measurements and fitted curves of composites with 25(orange), 50 (blue), 100 (green), 200 (red) ALD cycles and commercial 20 wt% Pt/C catalyst (black). The dots are the experimental data and the lines are the fitted curves. The insert is the equivalent circuit used for the fits for both the Mn3O4/CNTs and commercial 20 wt% Pt/C catalysts.

In order to further investigate the catalytic ORR mechanism and the charge transfer path at the interfaces between the different layers of the composite materials, electrochemical impedance spectroscopy (EIS) was carried out on samples prepared with 25, 50, 100 and 200 Mn_3O_4 ALD cycles at half-wave potential (0.71 V), which is located in the mixed diffusion-controlled region. Hence, both the charge transfer and mass transfer information can be acquired (**Figure 7**). The EIS are composed by a short straight line at high frequency and two separated semi-cycles. The straight line at high frequency is due to the coupling of the distributed ionic resistance and distributed capacitance in the catalyst layer[31] and the two semi-cycles are attributed to the charge transfer and mass transfer, respectively.[32] The negligible straight line indicates the minimized catalyst layer resistance.[31-32] The EIS of Pt/C shows only one semi-circle because the time constants of these two reactions are close to each other.[32a] The fitting values are presented in **Table 1**. R_s is the internal resistance which is due to the setup and is basically independent on the catalyst material. R_1 corresponds to the charge transfer resistance, which almost monotonically increases with the increase of the number of ALD cycles due to the increase of the thickness of the low conducting Mn_3O_4 coating. The samples with 25 and 50 ALD cycles exhibit the lowest charge transfer resistance pointing to the low polarization resistance of these samples, which is also in agreement with the interpretation of the Tafel plots (see above). R_2 corresponds to the mass transfer occurring at the interface between the catalyst and the liquid electrolyte and does not vary significantly, except for the sample with 25 ALD cycles. The much higher R_2 of the latter proves that 25 ALD cycles are not

sufficient for the fabrication of a good quality and conformal Mn_3O_4 coating onto the surface of the substrate, in agreement with the results discussed above (cf. **Figure SI-3**). This leads to an inefficient mass transfer at the solid-liquid interface. The EIS characteristic constants of the sample synthesized with 50 ALD cycles is comparable to Pt/C ORR catalyst.[32] Moreover, the characteristic time constant for the charge transfer (R_1*Q_1) of samples with 50, 100 and 200 ALD cycles stays constant, and is significantly lower than for the sample with 25 ALD cycles, which proves the high quality of the coating and the good contact between the carbon substrate and the Mn_3O_4 layer.[33] Last but not the least, the charge transfer resistance of the 50 ALD cycle sample is similar to the one of commercial 20 wt% Pt/C catalyst. This result further confirms that the 50 ALD cycles sample exhibits a polarization resistance similar to state of the art Pt/C.

Table 1. Fitting value of EIS with different ALD cycles at half-wave potential using Pt/C as reference.

	*R*s(Ω)	R_1 (Ω)	Q_1 (10^{-3})	N_1	R_2(Ω)	Q_2(10^{-3})	N_2
25 ALD cycles	72.8	184.4	0.33	0.8	616.4	0.8	1.0
50 ALD cycles	79.0	176.5	0.21	0.8	297.2	1.49	1.0
100 ALD cycles	74.5	204.0	0.16	0.8	264.0	2.28	1.0
200 ALD cycles	68.1	345.4	0.11	0.7	314.8	1.00	0.9
Pt/C	73.8	134.6	0.81	0.8	179.6	0.84	1.0

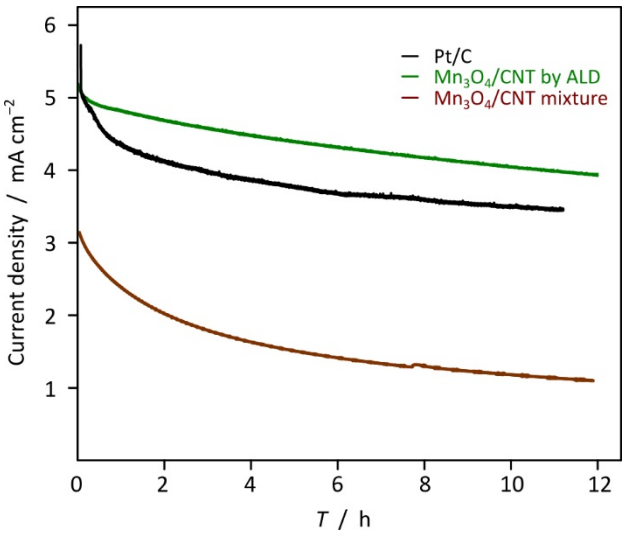

Figure 8. Chronoamperometric responses of Mn_3O_4/CNTs composite with 100 ALD cycles. The current density is recorded at a potential of 0.58 V (vs. RHE), Pt/C (black), Mn_3O_4/CNTs by ALD (green) and Mn_3O_4/CNTs mixture (brown).

The stability of the Mn_3O_4/CNTs composite is determined by chronoamperometric measurement in 0.1 M KOH at 0.58 V (**Figure 8**). The Mn_3O_4/CNTs composite synthesized by ALD exhibits significant higher stability compared to a physical mixture of Mn_3O_4 nanoparticles and CNTs due to the formation of a stable chemical bonding between the Mn_3O_4 deposited by ALD and the surface of the CNTs.[13a] Indeed, the Mn_3O_4/CNTs composite after 12 h sustain almost 80% of the initial current density. On the other hand, after 12 h the physical mixture and the reference Pt/C can only deliver 30% and 70% of their original current density, respectively due to the material corrosion in alkaline

solutions.[10, 30] Moreover, TEM images of the electrode materials after 12 h chronoamperometric measurements confirm that Mn_3O_4 particles are still present on the surface of the nanotubes (**Figure SI-5**). These findings demonstrate that the enhanced stability of the Mn_3O_4/CNTs composites is due to the peculiarity of the ALD technique allowing to grow conformal and covalently bonded metal oxide coatings onto high aspect ratio supports. Moreover, the higher stability of our samples suggests that a conformal coating also at least partially protects the carbon substrate from corrosion. These peculiarities make ALD the technique of choice for synthesizing highly active and stable metal oxide electrocatalysts for the ORR.

Experimental Section

CNTs pre-treatment: The treatment of CNTs before ALD is reported previously.[34] 200 mg CNTs (PR-24, Pyrograf Products, Inc.) were dispersed in 100 mL concentrated nitric acid in a round bottom flask, and the dispersion was refluxed at 105°C with stirring for 6 h. The CNTs were washed with distilled water by redispersion and centrifugation cycles until the solution exhibits neutral pH. The oxidized CNTs were then collected and dried at 80°C under vacuum overnight.

Atomic layer deposition (ALD): The Mn_3O_4 ALD process was reported in our previous work.[32] $MeCpMn(I)(CO)_3$ (min.97%, Strem Chemicals, Inc.) was utilized as metal precursor, and kept at 80°C during deposition, ozone generated from a BMT803N ozone generator was used as the oxygen source. The growth per cycle of Mn_3O_4 onto CNTs is approx. 0.034 nm. In this work, the deposition of Mn_3O_4 on CNTs was carried out onto 10 mg of oxidized CNTs. The CNTs were dispersed in 2 mL ethanol by ultra-sonication for 15 minutes. The dispersion was drop-casted on a 12 cm*12 cm well cleaned aluminium foil and dried under a nitrogen flow. The depositions were carried out with an ARRADIANCE GEMStar-6 commercial reactor using argon as the carrier gas. The manifold of the metal precursor was maintained at 130°C to inhibit possible condensation of the precursor. Pulse time (t_1), exposure time (t_2) and purge time (t_3) are 0.5 s, 30 s and 20 s, for $MeCpMn(I)(CO)_3$ and 1 s, 20 s and 20 s for ozone, respectively. After deposition, the CNTs were carefully wiped off from the aluminium foil and collected for the further characterization and electrochemical measurements.

Electrochemical measurements: All electrochemical measurements were carried out at 25°C on a Bio-Logic VMP3 electrochemical workstation with a three-electrode setup and a rotating disk electrode (RDE, AUTOLAB. B.V.). A Pt wire was used as the counter electrode and Ag/AgCl (3 M KCl) with double junction as reference electrode. All potentials reported were referred to the reversible hydrogen electrode (RHE) by adding a value of 0.21+0.059*pH V. The working electrode was a glassy carbon (GC) rotating disk electrode. 5 mg of Mn_3O_4/CNTs composite and 40 µL Nafion (5 wt%, Sigma-Aldrich) were dispersed in 960 µL of 1:1 v/v water/ethanol mixture for at least 30 min under sonication to form a homogeneous ink. Then 2 µL of the catalyst ink was drop-casted on a GC electrode followed by a rotational drying under 700 rpm for 20 min in air. The concentration of the Mn_3O_4/CNTs on the GC electrode for catalytic reaction was around 0.140 mg cm^{-2}. Linear sweep voltammetry (LSV) measurements were carried out in an O_2 saturated 0.1 M KOH aqueous solution with a scan rate of 10 mV s^{-1} between 0 V and 1 V with rotating rates at 400 rpm, 900 rpm, 1600 rpm and 2500 rpm. Prior to LSV measurements, five cyclic voltammetry (CV) cycles were acquired in an Ar-saturated and O_2-saturated 0.1 M KOH aqueous solution with the same scan rates. The capacitive contribution was determined by recording the CV measurements in the same potential window in

Ar-saturated solution. All CV and LSV measurements were iR-compensated to 85% during the measurements. Commercial 20% Pt/C catalyst and physical mixture of hausmannite Mn_3O_4 nanoparticles and CNTs (weight ratio of Mn_3O_4/CNTs is 1:1) were used for comparison with the Mn_3O_4/CNTs composites. The Mn_3O_4 nanoparticles were prepared by a wet chemical method using manganese(II) acetate as precursor, the nanoparticle size was ranging from 4-7 nm. Briefly, 433 mg manganese(II) acetate was mixed with 8.2 mL oleylamine and 0.4 mL water in 40 mL xylene. The mixture was diluted with 2.5 mL water and then stirred at 90°C for 2 hours. The nanoparticles were separated by centrifugation and washed with ethanol. The electrodes were prepared by the exact same procedure as the composites. 5 mg of the catalyst and 40 µL Nafion (5 wt%, Sigma-Aldrich) dispersed in 960 µL of 1:1 v/v water/ethanol and 2 µL of the ink were deposited on the glassy carbon electrode.

A Koutechy-Levich analysis was carried out to calculate the number of electrons transferred during the ORR on Mn_3O_4/CNTs catalyst.[35]

$$1/i_m = 1/i_k + 1/B_L\omega^{0.5} \quad (\mathbf{1})$$

Where i_m is the measured current, i_k is the kinetic current from the electrochemical reactions and $B_L\omega^{0.5}$ is the mass transport current.

The electron transfer number n can be calculated from the inverse slope of the current from LSV at 10 mV s^{-1} (–0.33 V vs. Ag/AgCl in 3 M KCl) and the inverse square root of the rotation rate.

$$\text{Slope} = 1/B_L = 1/(0.62nFAD^{2/3}v^{-1/6}C_0) \quad (\mathbf{2})$$

Where n is the electron transfer number per oxygen molecule, F is the Faraday's constant, A is the surface area of the electrode, in this work it is 0.07069 cm^{-2}. D is the diffusion coefficient of oxygen in 0.1 M KOH (1.9 X 10^{-5} cm^2 s^{-1}). v is the kinematic viscosity (1.1 X 10^{-2} cm^2 s^{-1}). The oxygen concertation C_0 is 1.2 X 10^{-2} mol cm^{-3}, and the ω is the rotation speed in radians.

Electrochemical impedance spectroscopy (EIS) was conducted on a VMP-3 electrochemical workstation with an AC voltage amplitude of 5 mV, the frequency is from 100 KHZ to 0.01 HZ with 10 points per decade. The EIS of composites with 25, 50, 100, 200 ALD cycles were collected at the half-wave potential (0.71V) in an oxygen-saturated 0.1 M KOH solution at 1600 rpm. The electrodes were equilibrated at the corresponding bias potential for 30 s before starting the EIS.

Characterizations: A STOE MP X-ray diffractometer (XRD) operated at 40 kV, 100 mA with Molybdenum $K\alpha$ radiation (λ = 0.7094 Å) was used for structural analysis. The 2ϑ range was set from 5° to 55°. The morphology and structure were characterized by Philips CM200 LaB_6 transmission electron microscopy (TEM) at 200 kV. High resolution transmission electron microscopy images were obtained using a JEM-ARM200F (Jeol) double-corrected cold field emission TEM operated at 200 kV. The obtained composites powder was pressed onto a carbon tap for XPS measurements. X-ray photoelectron spectroscopy (XPS) was performed in an ultrahigh vacuum chamber using a JPS-9030 photoelectron spectrometer hemispherical energy analyzer and a nonmonochromatic Al $K\alpha$ ($h\nu$ = 1486.6 eV) X-ray source (1.2 eV resolution).

Conclusions

In this work, we demonstrated that by precisely tuning the atomic layer deposition (ALD) parameters it was possible to synthesize a metal oxide/CNTs composite material that showed a similar oxygen reduction reaction (ORR) mechanism, kinetics and even better stability than a state of the art Pt-based catalyst. 2-10 nm thick Mn_3O_4 films were deposited onto CNTs by an ALD process between $MeCpMn(I)(CO)_3$ and ozone at temperatures ranging from 150 to 275 °C. The best ORR activities were recorded for the highest crystalline films synthesized at 275°C, which exhibits a current density twice as large in the diffusion limited region and a more than 100 mv lower onset potential compared to bare CNTs. In particular, the thinnest conformal film (~2nm after 50 ALD cycles) shows not only a one-step four electrons mechanism, but also similar kinetics than Pt-based catalysts. The latter is attributed to the low polarization of the ultrathin coating that does not increase the resistivity of the electrode material. As a matter of fact, thicker coatings exhibit larger Tafel slopes than Pt/C due to an increase of the polarization caused by the decreasing of the conductivity of the electrode induced by a thicker and continuous coating with a low conductive material. Moreover, the metal oxide coating showed to protect, at least to a certain extent, the carbon support from undesired side reactions. All in all, the herein reported nanostructured materials synthesis concept, opens new possibilities in using low conductive metal oxide materials in electrocatalytic applications.

Acknowledgements

The authors thank Sebastian Wahl and Tino Nerger for providing the Mn_3O_4 nanoparticles and Prof. Dr. Klaus Rademann and Prof. Dongsheng Geng for fruitful discussions. Y.F. acknowledges the fellowship from the China Scholarship Council (CSC).

References

[1] a) M. Shao, Q. Chang, J.-P. Dodelet, R. Chenitz, *Chem. Rev.* **2016**, *116*, 3594; b) C. Zhu, H. Li, S. Fu, D. Du, Y. Lin, *Chem. Soc. Rev.* **2016**, *45*, 517.

[2] a) J. Zhang, M. B. Vukmirovic, Y. Xu, M. Mavrikakis, R. R. Adzic, *Angew. Chem., Int. Ed.* **2005**, *44*, 2132; b) J. Greeley, I. E. L. Stephens, A. S. Bondarenko, T. P. Johansson, H. A. Hansen, T. F. Jaramillo, J. Rossmeisl, I. Chorkendorff, J. K. Nørskov, *Nat. Chem.* **2009**, *1*, 552.

[3] J.-S. Lee, G. S. Park, H. I. Lee, S. T. Kim, R. Cao, M. Liu, J. Cho, *Nano Lett.* **2011**, *11*, 5362.

[4] Y. Meng, W. Song, H. Huang, Z. Ren, S.-Y. Chen, S. L. Suib, *J. Am. Chem. Soc.* **2014**, *136*, 11452.

[5] M. S. El-Deab, T. Ohsaka, *J. Electrochem. Soc.* **2006**, *153*, A1365.

[6] a) Z.-R. Tian, W. Tong, J.-Y. Wang, N.-G. Duan, V. V. Krishnan, S. L. Suib, *Science* **1997**, *276*, 926; b) M.-K. Song, S. Cheng, H. Chen, W. Qin, K.-W. Nam, S. Xu, X.-Q. Yang, A. Bongiorno, J. Lee, J. Bai, T. A. Tyson, J. Cho, M. Liu, *Nano Lett.* **2012**, *12*, 3483; c) K. Mette, A. Bergmann, J.-P. Tessonnier, M. Hävecker, L. Yao, T. Ressler, R. Schlögl, P. Strasser, M. Behrens, *ChemCatChem* **2012**, *4*, 851.

[7] J. Duan, S. Chen, S. Dai, S. Z. Qiao, *Adv. Funct. Mater.* **2014**, *24*, 2072.

[8] D. Yan, Y. Li, J. Huo, R. Chen, L. Dai, S. Wang, *Adv. Mater.* **2017**, *29*, 1606459.

[9] a) J. Xu, W. Huang, R. L. McCreery, *J. Electroanal. Chem.* **1996**, *410*, 235; b) R. J. Bowling, R. T. Packard, R. L. McCreery, *J. Am. Chem. Soc.* **1989**, *111*, 1217; c) B. Šljukić, C. E. Banks, R. G. Compton, *J. Iran. Chem. Soc.* **2005**, *2*, 1.

[10] a) W. Jin, H. Du, S. Zheng, H. Xu, Y. Zhang, *J. Phys. Chem. B* **2010**, *114*, 6542; b) A. A. Gewirth, M. S. Thorum, *Inorg. Chem.* **2010**, *49*, 3557.

[11] M. S. Dresselhaus, G. Dresselhaus, P. C. Eklund, A. M. Rao, *The Physics of Fullerene-Based and Fullerene-Related Materials*, Springer Netherlands, Dordrecht, **2000**.

[12] U. Schroeder, S. Jakschik, E. Erben, A. Avellan, S. P. Kudelka, M. Kerber, A. Link, A. Kersch, *ECS Trans.* **2006**, *1*, 125.

[13] a) C. Marichy, N. Pinna, *Coord. Chem. Rev.* **2013**, *257*, 3232; b) M.-G. Willinger, G. Neri, E. Rauwel, A. Bonavita, G. Micali, N. Pinna, *Nano Lett.* **2008**, *8*, 4201; c) S. Boukhalfa, K. Evanoff, G. Yushin, *Energy Environ. Sci.* **2012**, *5*, 6872.

[14] J. W. Elam, J. A. Libera, T. H. Huynh, H. Feng, M. J. Pellin, *J. Phys. Chem. C* **2010**, *114*, 17286.

[15] a) R. L. Puurunen, *J. Appl. Phys.* **2005**, *97*, 121301; b) S. M. George, *Chem. Rev.* **2010**, *110*, 111.

[16] a) N. Pinna, M. Knez, *Atomic Layer Deposition of Nanostructured Materials*, Wiley-VCH Verlag GmbH & Co. KGaA, **2011**; b) M. C. Schwille, T. Schössler, J. Barth, M. Knaut, F. Schön, A. Höchst, M. Oettel, J. W. Bartha, *J. Vac. Sci. Technol., A* **2017**, *35*, 01B118; c) R. L. Puurunen, F. Gao, in *2016 14th International Baltic Conference on Atomic Layer Deposition (BALD)*, **2016**, 20-24.

[17] C. Marichy, M. Bechelany, N. Pinna, *Adv. Mater.* **2012**, *24*, 1017.

[18] R. Liu, Y. Lin, L.-Y. Chou, S. W. Sheehan, W. He, F. Zhang, H. J. M. Hou, D. Wang, *Angew. Chem.* **2011**, *123*, 519.

[19] M. K. S. Barr, L. Assaud, Y. Wu, C. Laffon, P. Parent, J. Bachmann, L. Santinacci, *Electrochim. Acta* **2015**, *179*, 504.

[20] K. L. Pickrahn, S. W. Park, Y. Gorlin, H.-B.-R. Lee, T. F. Jaramillo, S. F. Bent, *Adv. Energy Mater.* **2012**, *2*, 1269.

[21] R. M. Silva, G. Clavel, Y. Fan, P. Amsalem, N. Koch, R. F. Silva, N. Pinna, *Adv. Mater. Interfaces* **2016**.

[22] a) E. S. Ilton, J. E. Post, P. J. Heaney, F. T. Ling, S. N. Kerisit, *Appl. Surf. Sci.* **2016**, *366*, 475; b) A. Guimin, Y. Ping, X. Meijun, L. Zhimin, M. Zhenjiang, D. Kunlun, M. Lanqun, *Nanotechnology* **2008**, *19*, 275709.

[23] a) J. W. Lee, A. S. Hall, J.-D. Kim, T. E. Mallouk, *Chem. Mater.* **2012**, *24*, 1158; b) S. Ardizzone, C. L. Bianchi, D. Tirelli, *Colloids Surf., A* **1998**, *134*, 305.

[24] a) T. Sharifi, G. Hu, X. Jia, T. Wågberg, *ACS Nano* **2012**, *6*, 8904; b) Y. He, D. Gehrig, F. Zhang, C. Lu, C. Zhang, M. Cai, Y. Wang, F. Laquai, X. Zhuang, X. Feng, *Adv. Funct. Mater.* **2016**, *26*, 8255.

[25] a) K. Gong, F. Du, Z. Xia, M. Durstock, L. Dai, *Science* **2009**, *323*, 760; b) N. Levy, A. Mahammed, A. Friedman, B. Gavriel, Z. Gross, L. Elbaz, *ChemCatChem* **2016**, *8*, 2832.

[26] Y. Gorlin, C.-J. Chung, D. Nordlund, B. M. Clemens, T. F. Jaramillo, *ACS Catal.* **2012**, *2*, 2687.

[27] X. C. Yan, Y. Jia, F. Chen, Z. H. Zhu, X. D. Yao, *Adv. Mater.* **2016**, *28*, 8771.

[28] X. Lv, W. Lv, W. Wei, X. Zheng, C. Zhang, L. Zhi, Q.-H. Yang, *Chem. Commun.* **2015**, *51*, 3911.

[29] a) J. Xiao, L. Wan, X. Wang, Q. Kuang, S. Dong, F. Xiao, S. Wang, *J. Mater. Chem. A* **2014**, *2*, 3794; b) M. Nunes, I. M. Rocha, D. M. Fernandes, A. S. Mestre, C. N. Moura, A. P. Carvalho, M. F. R. Pereira, C. Freire, *RSC Adv.* **2015**, *5*, 102919; c) C. F. Zinola, A. M. Castro Luna, W. E. Triaca, A. J. Arvia, *J. Appl. Electrochem.* **1994**, *24*, 531; d) T. Shinagawa, A. T. Garcia-Esparza, K. Takanabe, *Sci. Rep.* **2015**, *5*, 13801.

[30] Y. Liang, Y. Li, H. Wang, J. Zhou, J. Wang, T. Regier, H. Dai, *Nat Mater* **2011**, *10*, 780.

[31] T. E. Springer, T. A. Zawodzinski, M. S. Wilson, S. Gottesfeld, *J. Electrochem. Soc.* **1996**, *143*, 587.

[32] a) R. K. Singh, R. Devivaraprasad, T. Kar, A. Chakraborty, M. Neergat, *J. Electrochem. Soc.* **2015**, *162*, F489; b) X. Zheng, Z. Yang, J. Wu, C. Jin, J.-H. Tian, R. Yang, *RSC Adv.* **2016**, *6*, 64155.

[33] Q. Ni, D. W. Kirk, S. J. Thorpe, *ECS Trans.* **2015**, *66*, 15.

[34] J. Zhang, H. Zou, Q. Qing, Y. Yang, Q. Li, Z. Liu, X. Guo, Z. Du, *J. Phys. Chem. B* **2003**, *107*, 3712.

[35] A. J. Bard, R. F. Larry, *Electrochemical Methods: Fundamentals and Applications*, 2nd ed., Wiley, **2000**.